Hindawi Publishing Corporation
International Journal of Photoenergy
Volume 2014, Article ID 854217, 10 pages
http://dx.doi.org/10.1155/2014/854217

Research Article

Self-Assembly of TiO_2/CdS Mesoporous Microspheres with Enhanced Photocatalytic Activity via Hydrothermal Method

Sujing Yu, Juncheng Hu, and Jinlin Li

Key Laboratory of Catalysis and Materials Science of the State Ethnic Affairs Commission & Ministry of Education, South-Central University for Nationalities, Wuhan, Hubei 430074, China

Correspondence should be addressed to Juncheng Hu; junchenghuhu@hotmail.com

Received 3 April 2014; Accepted 29 April 2014; Published 2 June 2014

Academic Editor: Mei Li

Self assembly of TiO_2/CdS mesoporous microspheres was synthesized via hydrothermal method. The samples were characterized by X-ray powder diffraction (XRD), ultraviolet-visible diffuse reflectance spectroscopy (DRS), transmission electron microscopy (TEM), energy-dispersive spectroscopy analysis (EDS), high-resolution transmission electron microscopy (HRTEM), Brunauer-Emmett-Teller (BET), X-ray photoelectron spectroscopy (XPS), and photoluminescence spectra (PL). The as-synthesized TiO_2/CdS mesoporous microspheres showed superior photocatalytic activity for the degradation of RhB under either visible light or simulated sunlight irradiation; the 10 wt% TiO_2/CdS sample showed the best performance. Moreover, this catalyst showed improved stability, and the activity did not decrease significantly after four recycles. The heterojunction between TiO_2 and CdS may be favorable for the transport of photoinduced electrons from CdS to TiO_2. In addition, the mesoporous structure could increase the utilization of light energy and facilitate the diffusion of reactants and products during the photocatalytic reaction.

1. Introduction

Textile and dye-related industries produce various organic pollutants, and these pollutants are very harmful to the surrounding environment [1]. In order to preclude the potential danger of recalcitrant organic dyes, many technologies have been developed to treat these pollutants [1]. Among these technologies, photocatalytic degradation technology has a lot of advantages, such as environmental friendliness, low energy consumption, low cost, and mild reaction conditions [2]. As an important chalcogenide semiconductor photocatalytic material, CdS attracts more and more attention because of its unique nature [3]. For example, CdS has an intrinsic narrow band gap (2.4 eV), it can be excited by visible light and has high utilization of solar light, and, moreover, it is low-cost in wastewater treatment [4, 5]. Nevertheless, there are still several negative factors that limit the utilization of CdS, such as the high recombination rate of the photogenerated electron- (e^--) hole (h^+) pairs resulting in less electrons (and holes) reaching the interface between photocatalyst and liquid, where the photocatalytic degradation takes place [6]. Moreover, CdS prepared by previous researchers was prone to photocorrosion by the photogenerated holes [7] in the photocatalytic reaction. On the other hand, nanosized CdS is easily aggregated to larger particles; thus, its surface area is reduced and the recombination rate of photoinduced electron-hole pairs becomes higher [2, 8, 9]. In order to overcome these shortcomings, attempts have been made to improve the stability of the metal sulfide [10–12]. Coupling CdS with another wide band gap semiconductor to form heterostructures becomes a hot topic in recent years. In such semiconductor heterostructures, the electrons generated in the CB of CdS can be injected into that of wide band gap semiconductor, which can inhibit the recombination rate of the electrons and holes pairs. Among some wide band gap semiconductors, TiO_2 is a desirable candidate in photocatalysis thanks to its suitable band gap (3.2 eV) and excellent optical property [13]; for example, TiO_2 is commonly used as photocatalyst because it is stable, nontoxic, and cheap. However, the following inherent drawbacks greatly restrict the practical application of naked TiO_2. Firstly, it can only be excited by UV light because of its large band gap (3.2 eV), which meant that only a small fraction of solar energy (3–5%) can be utilized [14, 15]. Secondly, the recombination rate of

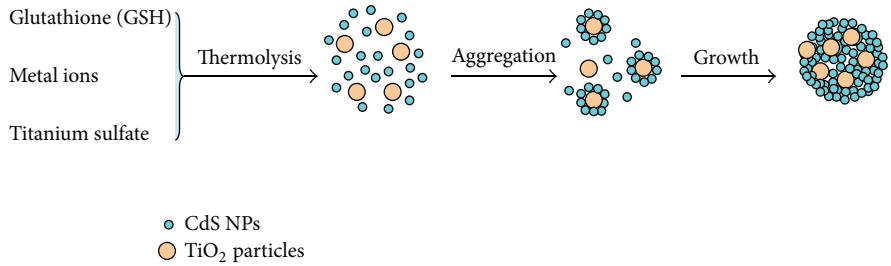

Scheme 1: Illustration of the preparation process of the TiO_2/CdS mesoporous microspheres.

the photogenerated electron- (e^--) hole (h^+) pairs is high [14, 16]. TiO_2/CdS semiconductor heterostructures (or composite microspheres) can compensate the disadvantages of the individual components to induce some synergistic effects, such as efficient charge separation and migration, expanded visible light response, and the improved photostability [17]. Because the CB position of CdS is 0.5 eV more negative than that of TiO_2, the electrons in CdS illuminated by visible light can be injected into TiO_2 easily, the charge separation efficiency of CdS is highly improved, and thus the photocatalytic activity is highly improved.

TiO_2/CdS composite photocatalysts have been widely studied to decompose contaminants effectively in recent years [18]. These TiO_2/CdS composite photocatalysts have different morphologies, for example, nanoparticle, nanorod, nanotube, film, and so on [17, 19–21]; however, most of these composite photocatalysts were synthesized at high temperature, typically from 300 to 600°C [1, 17, 22–24], which lead to the increasing of the crystallite size and the decrease of the specific surface area; these factors can result in the reducing of photocatalytic activity [25]. The synthesis of TiO_2/CdS composition with high visible-light photocatalytic activity at low temperature is of great importance.

In the present work, TiO_2/CdS composite microspheres were synthesized via self-assembly method at a relatively low temperature of 200°C; the preparation process was summarized in Scheme 1. The glutathione (GSH) was used as sulfur source [26]; titanium sulfate was used as the precursor of TiO_2. At an elevated temperature, the primary CdS nanoparticles were formed by thermolysis of metal ions GSH, which could assemble around the TiO_2 NPs driven by minimization of interfacial energy, and the fresh-formed crystalline CdS nanoparticles were unstable because of their high surface energy. The continuous aggregation process occurs at the TiO_2-CdS and CdS-CdS interface ultimately resulted in the formation of TiO_2/CdS composite microspheres [27]. This method had many advantages. On one hand, the synthesis temperature was relatively low; thus, the crystallite size was small with larger specific surface area, which could supply more reaction active sites where organic molecules and intermediate products were adsorbed. On the other hand, the morphology of the product was mesoporous microspheres. Mesoporous microspheres had higher conductivities and electron mobilities and higher specific surface area; the multiple reflection light in the mesoporous structure may lead to higher efficiency of light utilization. These factors can contribute to the improvement of the photocatalytic activity. Moreover, the self-assembly method was very simple and easy. We have tested the photocatalytic activity of the as-synthesized TiO_2/CdS mesoporous microspheres by the degradation of RhB. The TiO_2/CdS mesoporous microspheres showed better photocatalytic activity than pure CdS and TiO_2under visible light, which was attributed to the impact of TiO_2 on CdS. When using simulated sunlight irradiation, the photocatalytic activity of the TiO_2/CdS mesoporous microspheres was improved remarkably; it was superior to the commercial Degussa P25 TiO_2, which indicated that the as-synthesized TiO_2/CdS mesoporous microspheres have efficient utilization of solar energy. Some factors may lead to the result; for example, the heterojunction between TiO_2 and CdS may be favorable for the transport of photoinduced electrons from CdS to TiO_2. Furthermore, both $TiO_2$and CdS can be excited by simulated sunlight; moreover, $TiO_2$and CdS could interact with each other.

2. Experiment Section

2.1. Materials and Sample Preparation. All chemicals were of analytical grade (purchased from Aladdin) and were used as received without further purification. In a typical synthesis, 5.5 mmol $Cd(NO_3)_2{\cdot}4H_2O$ and 5.5 mmol glutathione (GSH, $C_{10}H_{17}N_3O_6S$) were dissolved in 205 mL deionized water to form a clear solution. Then 25 mL methanol was added to the clear solution. One hour later, 0.4 g titanium sulfate was added to the solution under vigorous stirring. After being continuously stirred for 24 h, the solution was transferred into an autoclave with a quartz inline. The autoclave was purged with nitrogen for 3 times, and then a pressure of 1 MPa was imposed into the autoclave. The solution was heated to 200°C and maintained for several hours. Subsequently, the autoclave was cooled to room temperature naturally. The obtained samples were filtered, washed with ethanol for several times, and then dried at 60°C in an oven overnight. The same procedures were applied to synthesize pure CdS and pure TiO_2. When the reaction time was 10 h, the as-synthesized samples with different weight ratios of 0.1 : 0.9, 0.12 : 0.88, and 0.07 : 0.93 of TiO_2 and CdS were denoted as S1-10, S2, S3, respectively. When the weight ratio of TiO_2 and CdS was 1 : 9, the reaction time was 5 h, 20 h, and the samples were denoted as S1-5, S1-20, respectively.

2.2. Characterization. The crystalline structure of the catalysts was characterized by power X-ray diffraction (XRD) using Cu Kα radiation. The scanning rate was 0.05°/s within 2θ range from 10° to 80°. The morphologies and size of the samples were studied by transmission electron micrograph (TEM) and high resolution transmission electron microscopy (HRTEM) analyses using a Tecnai G20 (FEI Co., Holland) microscope operated at accelerating voltage of 200 kV. Energy dispersive spectrum analysis (EDS) system was connected to the TEM. The ultraviolet-visible diffuse reflectance spectroscopy (DRS) was collected using a Shimadzu UV-2450 spectrophotometer from 200 nm to 800 nm using $BaSO_4$ as background. X-ray photoelectron spectroscopy (XPS) was recorded on a VG Multilab 2000 (VG Inc.) photoelectron spectrometer using monochromatic Al-K radiation under vacuum at 2×10^{-6} Pa. All of the binding energies were referenced to the C_{1s} peak at 284.8 eV of the surface adventitious carbon. The photoluminescence (PL) spectra of the samples were recorded with a PE LS55 spectrophotometer. The Brunauer-Emmett-Teller (BET) specific surface areas of the samples were evaluated on the basis of nitrogen adsorption isotherms using a Micromeritics ASAP 2020 gas adsorption apparatus (USA).

2.3. Photocatalytic Activity Measurement. The photocatalytic activity of the as-prepared samples was evaluated by the degradation of RhB (50 mL, 1×10^{-5} mol/L). The test was carried out under visible light and simulated sunlight irradiation of a 350 W Xe lamp, respectively. In a typical process, 50 mg of catalyst was suspended in the RhB solution. Then the suspension was magnetically stirred in dark for 3 h to ensure the establishment of an adsorption/desorption equilibrium between the organics and the catalyst, at given irradiation time interval, 3 mL solution was taken and centrifuged to remove the catalyst particulates. The filtrates were finally analyzed using a UV-vis spectrophotometer (UV-2450). As a comparison, the photocatalytic activities of degussa P25 were tested under the same experimental conditions.

2.4. Analysis of Hydroxyl Radicals $^{\bullet}OH$. The production of $^{\bullet}OH$ on the surface of the photocatalyst was detected by a photoluminescence (PL) method using coumarin as a probe molecule. Coumarin can readily react with $^{\bullet}OH$ to produce highly fluorescent product, 7-hydroxycoumarin. Experimental procedure was similar to the measurement of photocatalytic activity. Coumarin (50 mL, 5×10^{-4} M) and S1-10 (50 mg) were mixed under magnetic stirring for 3 h under dark conditions. Then, the suspension was irradiated under simulated sunlight irradiation. At given irradiation time intervals, the reaction solution was sampled and then centrifuged to measure the PL intensity around 454 nm excited by the wavelength of 332 nm.

3. Results and Discussion

Figure 1 showed the temporal evolution of the spectra during the photodegradation of RhB mediated by a series of synthetic samples under visible light of a 350 W Xe lamp with a 420 nm cut-off filter. As shown in Figure 1(a), with the addition of 50 mg mesoporous microspheres (S1-10), the degradation percentage was about 90% in 20 min. However, for TiO_2, P25, and CdS, the degradation percentage was about 22%, 58%, and 70%, respectively, in the same condition, which revealed that 10 wt% mesoporous microspheres showed superior photocatalytic activity. Moreover, Figure 1(b) revealed that when the reaction time was 10 h, the mesoporous microspheres showed better photocatalytic activity. A series of experiments shown in Figure 1 demonstrated that the S1-10 sample displayed the best photocatalytic activity. It should be noted that the degradation of RhB by pure TiO_2 was attributed to the sensitization of RhB (as a dye) [1]. When $TiO_2$was introduced into pure CdS, the photocatalytic activity was improved under visible light. The photocatalytic activity of the several samples under simulated sunlight irradiation was also tested, as shown in Figure 2. In 10 min, the degradation percentage of RhB by pure TiO_2 and CdS was about 74% and 70%, respectively. But when TiO_2/CdS mesoporous microspheres (S1-10) were used as photocatalyst in the same condition, the RhB was completely degraded. For comparison, the photocatalytic activity of P25 was also tested. Obviously, TiO_2/CdS mesoporous microspheres showed better photocatalytic activity than P25.

The X-ray diffraction (XRD) measurement was employed to identify the phase structure of the as-prepared samples. As shown in Figure 3, the XRD pattern of the as-prepared CdS showed some sharp peaks at 2θ value of 24.6°, 26.3°, 28.0°, 43.3°, 47.7°, and 51.6°, which were assigned to the CdS (JCPDS number 75-1545) greenockite phase (100), (002), (101), (110), (103), and (112), respectively. The main peaks of S1-10 were close to CdS, which illustrated that the main component of S1-10 was CdS, but the peaks of TiO_2did not appear; some factors may lead to the result. For instance, the peak position of pure CdS and TiO_2 was close; the peaks of TiO_2 may be hidden. For example, the (100) peak of greenockite phase CdS might overlap with the primary characteristic peak of TiO_2at approximately 24.4° (JCPDS number 71-1169). In addition, TiO_2 was little, the main component was CdS, and TiO_2 dispersed well among CdS; thus CdS may be densely coated on the surface of TiO_2, which leads to the weak peaks of TiO_2. Moreover, compared to S1-5 and S1-20, the diffraction peaks of S1-10 became sharper and stronger; it is well reported that the increase in the crystallinity of semiconductor photocatalysts can usually lead to an enhancement of organic pollutants photodegradation since the crystallinity would mean few defects acting as the recombination centers for photogenerated electrons and holes [28, 29].

S1-10 was selected for analysis of the microscopic structure because of its high photocatalytic activity. Firstly, the morphology of S1-10 shown in Figures 4(a) and 4(b) demonstrated that the as-synthesized samples were mesoporous microspheres; the size was about 0.8 μm. It was attributed to the mixed stack of CdS and TiO_2[17]. The HRTEM image shown in Figure 4(c) indicated that the spacing of 0.316 nm and 0.336 nm corresponds to the (101) and (002) facet of greenockite CdS, while the spacing (0.354 nm) of (101) facet of anatase TiO_2 was also clearly observed. Additionally,

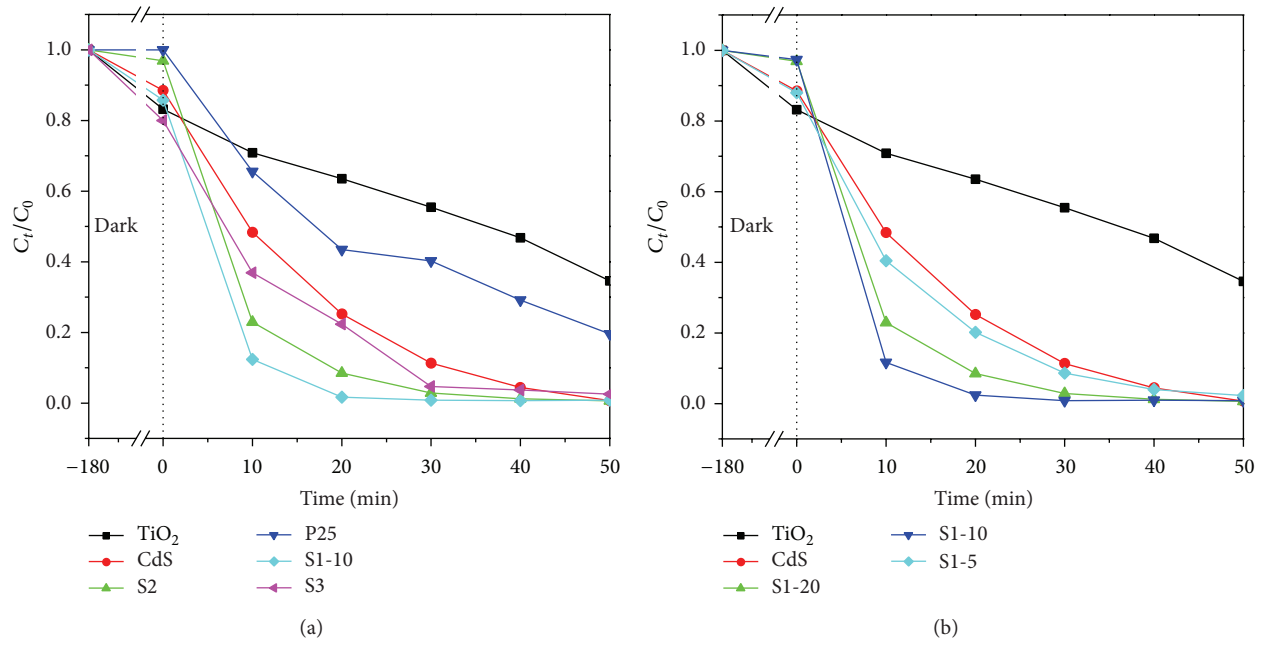

FIGURE 1: C_t/C_0 versus time curves of RhB photodegradation under visible light ($\lambda > 420$ nm) irradiation. (a) S1-10: 10 wt% TiO_2/CdS (10 h), S2: 12 wt% TiO_2/CdS (10 h), and S3: 10 wt% TiO_2/CdS (10 h); (b) S1: 10 wt% TiO_2/CdS (10 h), S1-5: 10 wt% TiO_2/CdS (5 h), and S1-20: 10 wt% TiO_2/CdS (20 h).

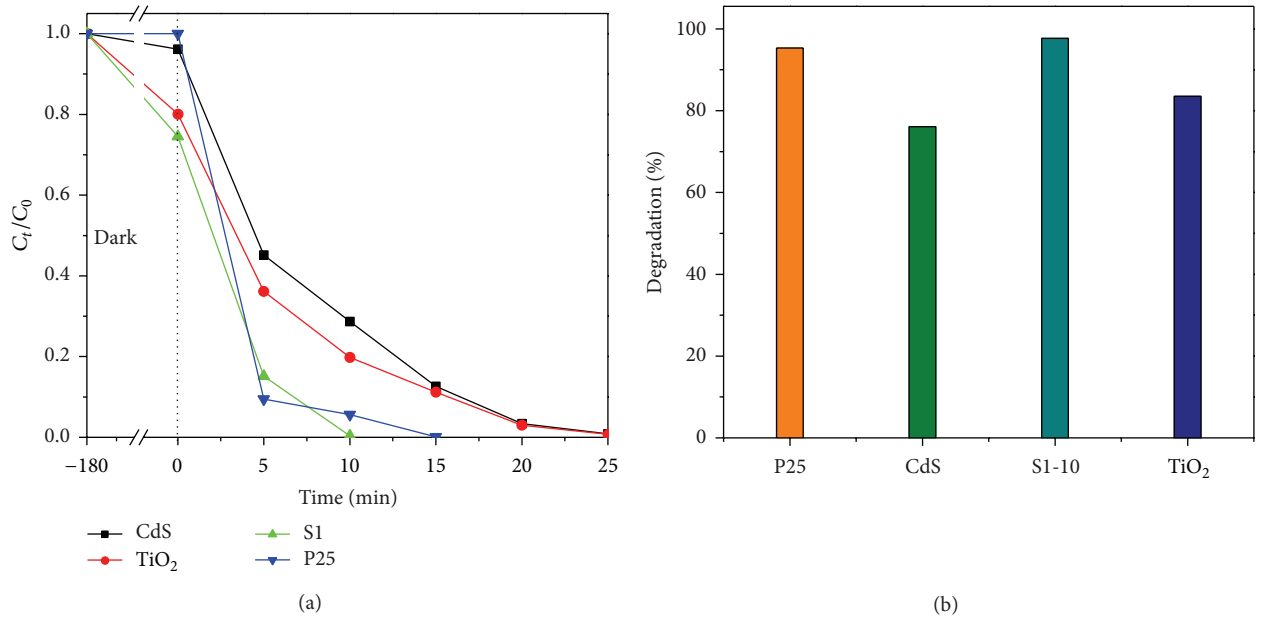

FIGURE 2: (a) C_t/C_0 versus time curves of RhB photodegradation under simulated sunlight irradiation by CdS, S1-10: 10 wt% TiO_2/CdS (10 h), TiO_2, and P25, respectively. (b) Comparison of the photocatalytic activity of P25, CdS, S1-10: 10 wt% TiO_2/CdS (10 h), and TiO_2, respectively, in 10 min.

the close contact between CdS and TiO_2 crystals in the HRTEM images revealed the existence of heterojunction in the interfacial area of the two substances [23]. These as-formed junctions were proved to contribute to facilitate interelectron transfer between the two components, which could improve the charge separation; thus the photocatalytic activity of the TiO_2/CdS mesoporous microspheres could improve significantly [24]. The EDS data in Figure 4(d) for the sample (S1-10) showed that the sample was composed of S, Cd, Ti, and O. The element molar ratio of Cd : S was close to 1 : 1, and their total weight percentage was 90%, which agreed well with the as-synthesized sample.

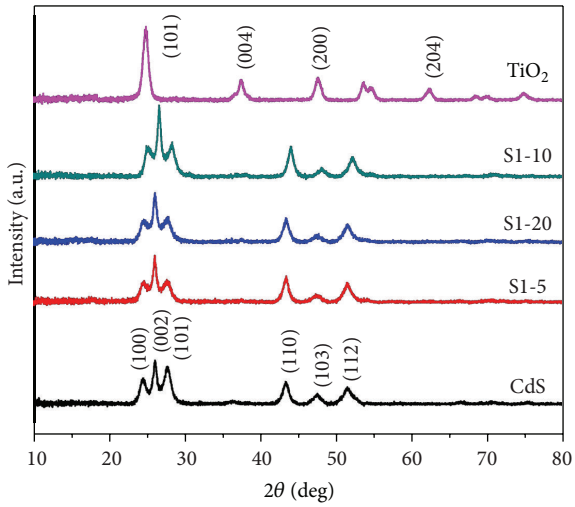

FIGURE 3: XRD patterns of CdS, S1-10: 10 wt% TiO_2/CdS (10 h), S1-5: 10 wt% TiO_2/CdS (5 h), S1-20: 10 wt% TiO_2/CdS (20 h), and TiO_2, respectively.

The X-ray photoelectron spectroscopy (XPS) was carried out to further determine the chemical states of the prepared samples. Cd 3d core levels were shown in Figure 5(a); two peaks located at 411.3 and 404.6 eV corresponded to the Cd $3d_{3/2}$ and Cd $3d_{5/2}$peaks and were assigned to $Cd^{2+}$of CdS with a spin-orbit separation of 6.7 eV, consistent with the reported values [30]. The result indicated that the Cd 3d core levels of the TiO_2/CdS mesoporous microspheres (S1-10) were similar with that of pure CdS [17]. The S 2p spectrum of S1-10 in Figure 5(b) included two individual peaks with respective binding energies 161.0 and 162.2 eV; the peak at about 161.0 eV could be assigned to the S atoms bonded to Ti atoms, which corresponded to S $2p_{3/2}$ of TiS_2 [31]. Meanwhile, the peak at about 162.2 eV could be assigned to the S atoms bonded to Cd atoms, which corresponded to S $2p_{3/2}$ of CdS [30]. Figure 5(c) showed the peak positions of Ti 2p. Two peaks located at 458.3 and 464.0 eV corresponded to Ti $2p_{3/2}$ and Ti $2p_{1/2}$ of Ti^{4+} in TiO_2 [32–34]. Because of the formation of Ti–S bonds, the peaks of Ti 2p shifted to a lower energy. Moreover, the asymmetric band of O 1s of TiO_2/CdS composite microspheres samples can be fitted into two peaks in Figure 5(d). The peak at about 529.6 eV was assigned to the crystal lattice oxygen of Ti–O, and the peak at about 530.8 eV could be assigned to the hydroxyl oxygen [28, 35].

In order to determine the optical properties of the samples, the UV-vis diffuse reflectance spectra (DRS) of CdS, TiO_2, and the TiO_2/CdS mesoporous microspheres (S1-10) were tested. Figure 6 showed that the visible-light absorption capacity of the TiO_2/CdS mesoporous microspheres was decreased compared with pure CdS, because $TiO_2$was insensitive to visible light. Moreover, there was another onset around 390 nm, which was caused by TiO_2, because TiO_2 has excellent absorption properties in the ultraviolet region. The TiO_2/CdS mesoporous microspheres (S1-10) showed better photocatalytic activity although the light absorption capacity of the TiO_2/CdS mesoporous microspheres was decreased and thus may result from the fact that, in TiO_2/CdS heterojunctions, the electrons generated in the CB of CdS can be injected into that of TiO_2; thus, the recombination of photoelectrons and holes could be effectively inhibited, which was favorable for the enhancement of the photocatalytic activity.

To study the role of TiO_2 in TiO_2/CdS mesoporous microspheres for the enhancement of photoactivity, the surface area and porosity of TiO_2/CdS mesoporous microspheres (S1-10) had been investigated using nitrogen adsorption-desorption measurements. As shown in Figure 7, TiO_2/CdS mesoporous microspheres exhibited a type IV isotherm according to the IUPAC classification, indicating a mesoporous structure. The pore-size distribution obtained from the isotherm revealed that the pores were about 34 nm in diameter. These pores could promote rapidly diffusion of the reactants and products during the photocatalytic reaction and thus enhance the rate of the photocatalytic reaction. The BET specific surface area and pore volume of the as-synthesized samples were shown in Table 1, which revealed that BET specific surface of S1-10 (which showed the best photocatalytic activity) was not the largest. In addition, the pore volume of the as-synthesized the TiO_2/CdS mesoporous microspheres was analogous. The result suggested that the enhanced photocatalytic activity of TiO_2/CdS mesoporous microspheres compared with pure CdS cannot be ascribed to the change in surface area and porosity.

Charge separation and transfer efficiency played a significance role in enhancing photocatalytic activity; thus, testing the PL spectra of pure CdS and TiO_2/CdS mesoporous microspheres (S1-10) was necessary. The result was shown in Figure 8; pure CdS showed strong PL emission at about 530 nm under an excitation wavelength of 350 nm. When the TiO_2 was introduced, the PL intensity of the TiO_2/CdS mesoporous microspheres became much weaker, suggesting the longer lifetime of photogenerated charge carriers. In heterojunction, the photogenerated electrons that transferred from the CB of CdS to the CB of TiO_2 could effectively prevent the direct recombination of electrons and holes. The low recombination rate of electrons and holes was favorable for the improvement of photocatalytic activity of the TiO_2/CdS mesoporous microspheres [2].

For further insight into the photocatalytic mechanism and to study the involved active species in the photocatalytic process, the PL technique was employed to detect hydroxyl radicals $^{\bullet}OH$ on the surface of simulated sunlight illuminated S1-10 by using coumarin as a probe molecule. Figure 9 showed the changes in the PL spectra for 5×10^{-4} M coumarin solution with different irradiation times in the presence of S1-10. It was clearly seen that the PL intensity of photogenerated 7-hydroxycoumarin at about 454 nm (excited at 332 nm) increases with the increase of irradiation time. However, PL intensity did not change in the absence of light irradiation or catalyst; it indicated that the fluorescence was produced by chemical reaction of coumarin with $^{\bullet}OH$ generated on the surface of the catalysts during the photocatalytic process [26, 36], which revealed that the fast production of $^{\bullet}OH$ radicals and the highly accumulated $^{\bullet}OH$ radicals were one of the active oxygen species in the photocatalytic process.

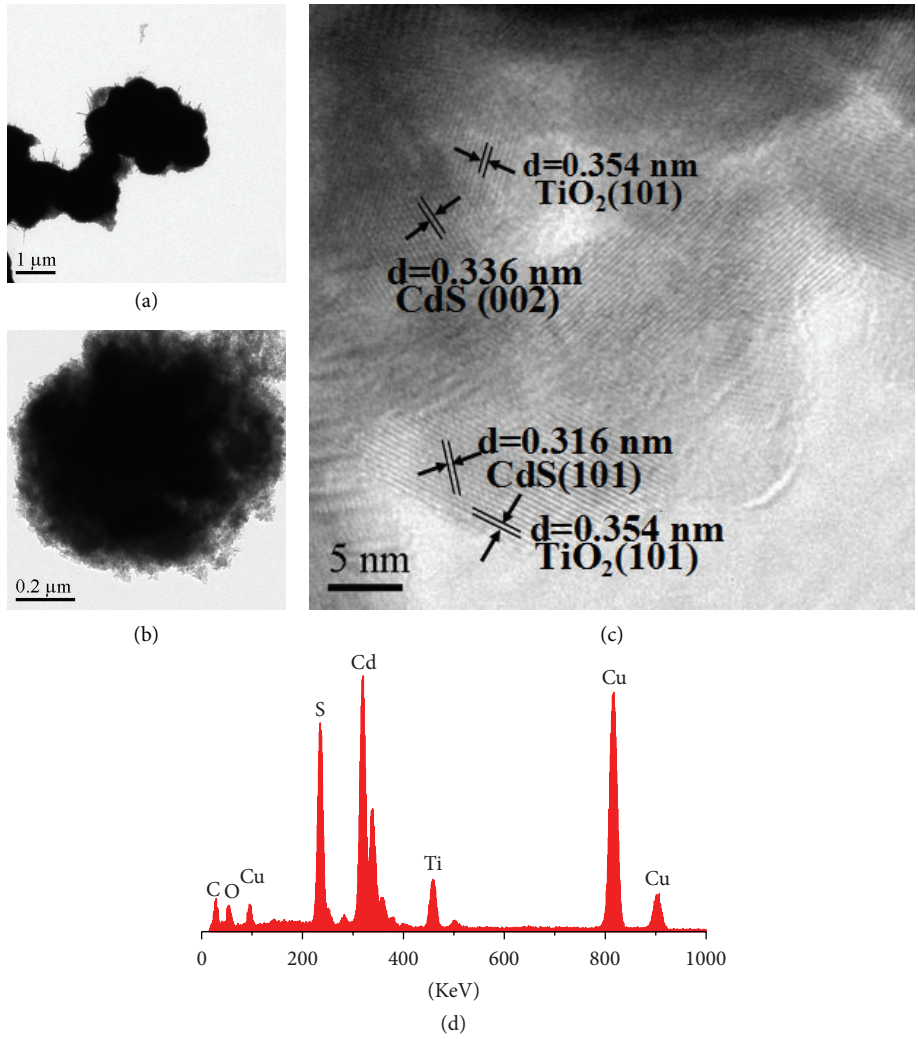

Figure 4: (a) and (b) TEM images of S1-10: 10 wt% TiO_2/CdS (10 h), (c) HRTEM images of S1-10, and (d) EDS image of S1-10.

Table 1: BET surface area and pore volume of the as-synthesized samples.

Sample	TiO_2 (wt.%)	Time (h)	S_{BET} (m^2/g)	Pore volume (cm^3/g)
CdS	0	10	25.4	0.07
TiO_2/CdS	10	10	54.9	0.16
TiO_2/CdS	12	10	62.7	0.14
TiO_2/CdS	7	10	47.3	0.12
TiO_2/CdS	10	20	57.2	0.15
TiO_2/CdS	10	5	51.0	0.13

The stability of the TiO_2/CdS mesoporous microspheres was tested by executing recycling reactions four times for the photodegradation of RhB under simulated sunlight irradiation. S1-10 was selected to be analyzed because it showed the best photocatalytic activity. Using the formula photodegradation efficiency (%) = $[(C_0 - C)/C_0] \times 100\%$, the photodegradation efficiency (%) could be calculated. C_0 is the initial concentration of RhB and C is the concentration of dye after photoirradiation. As shown in Figure 10, the degradation percentage of RhB does not change much after four cycles. The slight decrease may be caused by the wastage of photocatalyst when each sample was taken and centrifuged. It indicated that the TiO_2/CdS mesoporous microspheres were fairly stable and not photocorroded in the degradation of RhB [9].

4. Catalytic Mechanism

On the basis of the photodegradation results of RhB, a synergistic mechanism was speculated between CdS and

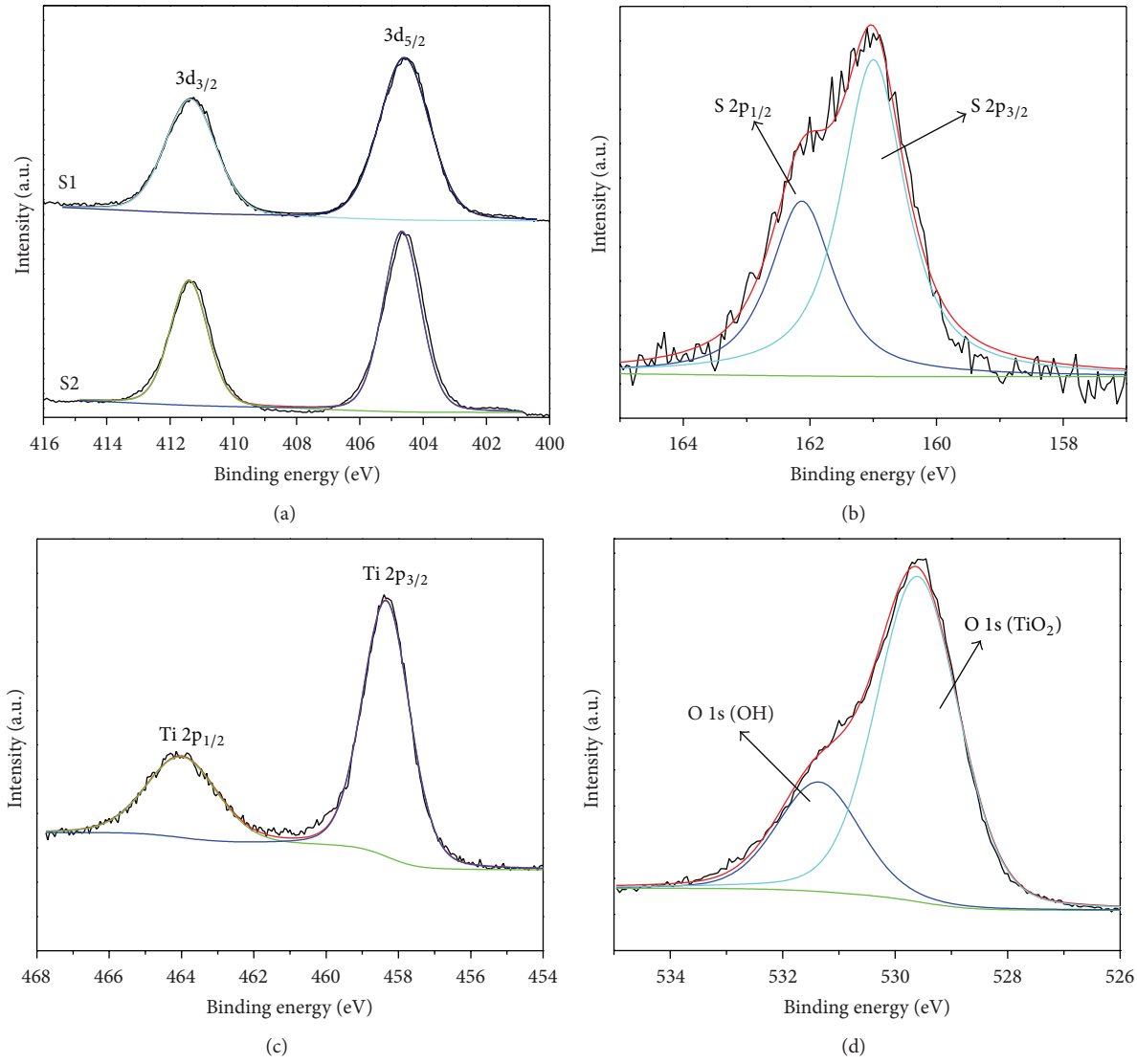

FIGURE 5: XPS analysis of as-obtained samples (a) Cd 3d of S1-10: 10 wt% TiO_2/CdS (10 h) and CdS; (b)S 2p; (c) Ti 2p; (d) O 1s of S1-10: 10 wt% TiO_2/CdS (10 h), respectively.

TiO_2 for photocatalysis of RhB. As shown in Scheme 2, when the light source is visible, TiO_2 cannot be excited, but some portion of RhB was degraded. It may be attributed to the photosensitizing and photoreduction process. Compared with pure CdS, the photocatalytic activity of TiO_2/CdS mesoporous microspheres (S1-10) photocatalysts for degrading RhB under visible light was improved, which may result from that TiO_2 had modification effect on CdS. In another case, when under simulated sunlight irradiation, the photocatalytic activity of the TiO_2/CdS mesoporous microspheres was much better than that of pure CdS and pure TiO_2 in the same condition. It provided further evidence that TiO_2 had modification effect on CdS; the electron transfer path may change. The conduction band (CB) and valence band (VB) potentials of CdS are at −1 eV and 1.42 eV [22, 37]; the CB edge potential of CdS (−1 eV) is more negative than that of TiO_2(−0.5 eV) [22, 37]; since heterojunction existed between CdS and TiO_2, the photoinduced electrons on the surface of CdS particle can transfer easily from the CB of CdS to that of TiO_2 via the well-developed interface [38]. Thus, photogenerated holes and electrons can stay on the surface of CdS and TiO_2, respectively; the recombination rate of electrons and holes pairs was reduced. Photogenerated holes could react with H_2O that adsorbed on the semiconductor surface; then hydroxyl radicals $^{\bullet}OH$ with high activity were generated. Meanwhile, the photogenerated electrons could generate $HO^{\bullet}$ and other active oxygen species such as $O_2^{-\bullet}$ by reacting with O_2 [28]. These active oxygen species could be directly involved in the photocatalytic redox reaction. Moreover, under the illumination of simulated sunlight, TiO_2 can be excited; the electrons (e^-) were photoexcited from the VB of TiO_2 to its CB, which also generate electron-hole pairs [35], and thus TiO_2 also contributed to the enhancement of photocatalytic activity. On the other hand,

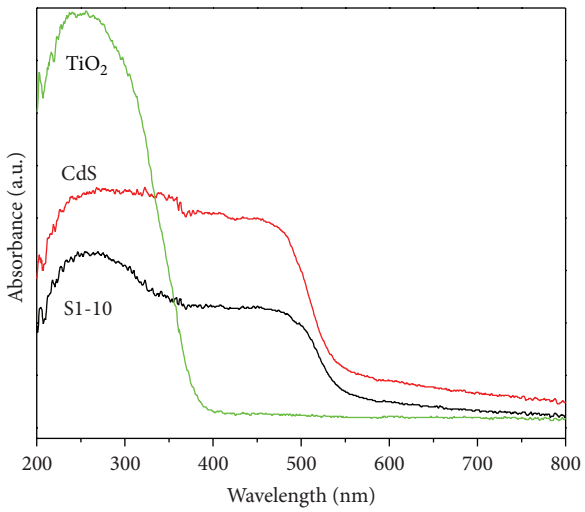

Figure 6: UV-vis diffuse reflectance spectra (DRS) of CdS, S1-10: 10 wt% TiO_2/CdS (10 h), and TiO_2, respectively.

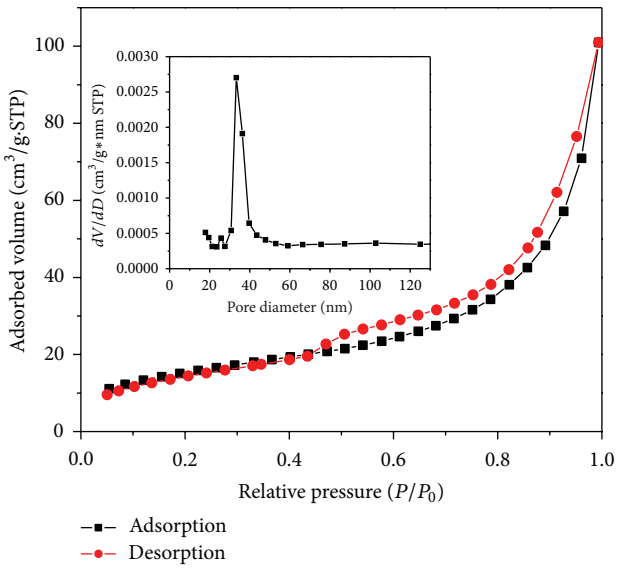

Figure 7: Adsorption/desorption isotherms of S1-10: 10 wt% TiO_2/CdS (10 h); inset is the corresponding pore size distribution curves.

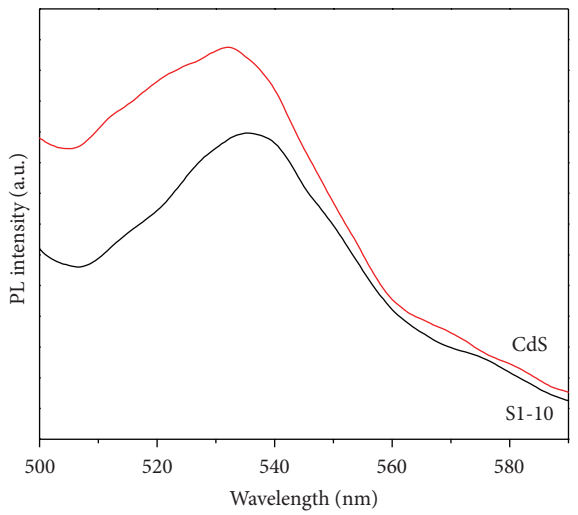

Figure 8: Photoluminescence (PL) spectra of CdS and S1-10: 10 wt% TiO_2/CdS (10 h).

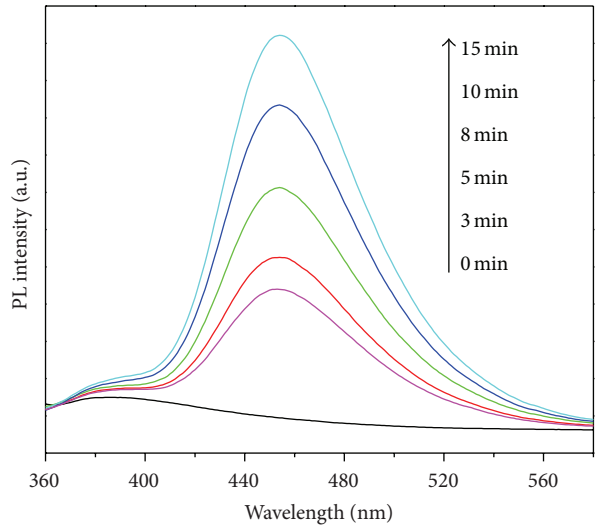

Figure 9: PL spectra changes observed during irradiated sunlight illumination of S1-10: 10 wt% TiO_2/CdS (10 h) in coumarin solution (excitation at 332 nm).

the adsorption of contaminant also played a role in the improvement of photocatalytic activity. The electron transfer rate became more efficient because of the close contact of RhB molecules and TiO_2/CdS mesoporous microspheres. Moreover, mesoporous structure can facilitate the diffusion of reactants and products during the photocatalytic reaction. The synergistic effect of the various factors leads to the enhancement of photocatalytic activity of the as-synthesized TiO_2/CdS mesoporous microspheres samples.

5. Conclusions

In summary, we have successfully synthesized CdS and TiO_2/CdS mesoporous microspheres via self-assembly method in the hydrothermal environment. The catalysts had superior photocatalytic activity in the degradation of RhB under either visible light or simulated sunlight irradiation. The 10 wt% TiO_2/CdS mesoporous microspheres showed the best excellent performance for removing organic pollutants. The mesoporous structure could increase the utilization of light energy and facilitate the diffusion of reactants and products during the photocatalytic reaction. Heterojunction in the interfacial area of $TiO_2$and CdS plays a key role in reducing the recombination rate of photon-generated carriers; thus, the activity and stability of the catalyst were promoted. We expect that the method and idea presented in this work will provide a new way for the construction of highly efficient photocatalysts not only for mesoporous microspheres, but also for other semiconductor materials.

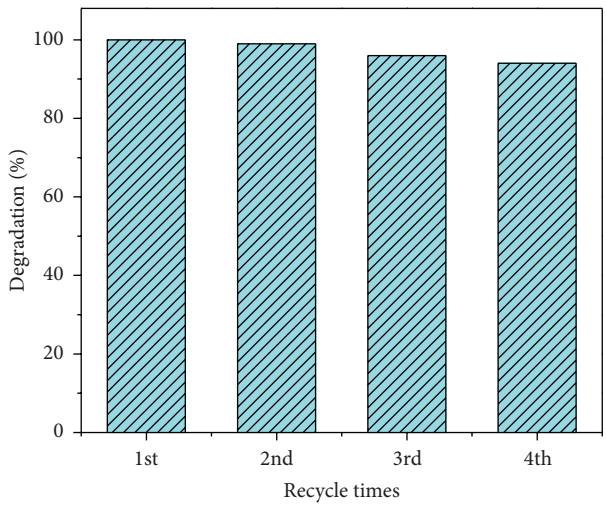

Figure 10: Degradation percentage of RhB in the presence of S1-10: 10 wt% TiO_2/CdS (10 h) under simulated sunlight irradiation for four recycles.

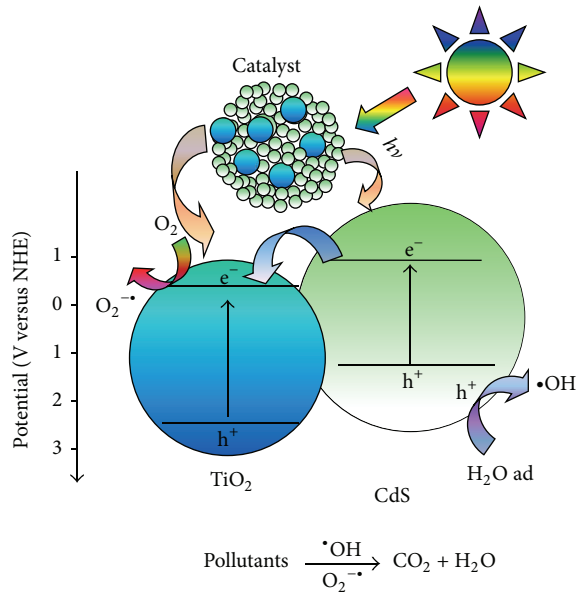

Scheme 2: The possible photocatalytic mechanism of TiO_2/CdS mesoporous microspheres.

Conflict of Interests

The authors declare that there is no conflict of interests regarding the publication of this paper.

Acknowledgments

This work was supported by Natural Science Foundation of Hubei Province (2013CFA089), Key Laboratory of Green Catalysis of Sichuan Institute of High Education (LYJ1108), and National Basic Research Program of China (Grant no. 2011CB211704). The project was also sponsored by the Scientific Research Foundation for the Returned Overseas Chinese Scholars, State Education Ministry (BZY09003), and Ministry of Human Resources and Social Security (BZY09012).
g

References

[1] J.-W. Shi, X. Yan, H.-J. Cui et al., "Low-temperature synthesis of CdS/TiO_2 composite photocatalysts: influence of synthetic procedure on photocatalytic activity under visible light," *Journal of Molecular Catalysis A: Chemical*, vol. 356, pp. 53–60, 2012.

[2] Q. Mi, J. C. Hu, M. Luo, Z. X. Huang, and J. L. Li, "CdS hollow spheres supported on graphene oxide sheets with enhanced photocatalytic activity," *Science of Advanced Materials*, vol. 5, pp. 1649–1657, 2013.

[3] J. Wu, S. Bai, X. Shen, and L. Jiang, "Preparation and characterization of graphene/CdS nanocomposites," *Applied Surface Science*, vol. 257, no. 3, pp. 747–751, 2010.

[4] A. Podborska, B. Gawel, L. Pietrzak et al., "Anomalous photocathodic behavior of CdS within the urbach tail region," *Journal of Physical Chemistry C*, vol. 113, no. 16, pp. 6774–6784, 2009.

[5] P. Kumar, P. K. Singh, and B. Bhattacharya, "Study of nano-CdS prepared in methanolic solution and polymer electrolyte matrix," *Ionics*, vol. 17, no. 8, pp. 721–725, 2011.

[6] D. Kannaiyan, E. Kim, N. Won et al., "On the synergistic coupling properties of composite CdS/TiO_2 nanoparticle arrays confined in nanopatterned hybrid thin films," *Journal of Materials Chemistry*, vol. 20, no. 4, pp. 677–682, 2010.

[7] D. Meissner, R. Memming, and B. Kastening, "Photoelectrochemistry of cadmium sulfide. 1. Reanalysis of photocorrosion and flat-band potential," *The Journal of Physical Chemistry*, vol. 92, no. 12, pp. 3476–3483, 1988.

[8] Y. Liu, Y. Hu, M. Zhou, H. Qian, and X. Hu, "Microwave-assisted non-aqueous route to deposit well-dispersed ZnO nanocrystals on reduced graphene oxide sheets with improved photoactivity for the decolorization of dyes under visible light," *Applied Catalysis B: Environmental*, vol. 125, pp. 425–431, 2012.

[9] W. Li, X. Cui, P. Wang, Y. Shao, D. Li, and F. Teng, "Enhanced photosensitized degradation of rhodamine B on CdS/TiO_2 nanocomposites under visible light irradiation," *Materials Research Bulletin*, vol. 48, no. 9, pp. 3025–3031, 2013.

[10] X. Zong, H. Yan, G. Wu et al., "Enhancement of photocatalytic H_2 evolution on CdS by loading MoS_2 as cocatalyst under visible light irradiation," *Journal of the American Chemical Society*, vol. 130, no. 23, pp. 7176–7177, 2008.

[11] C. M. Janet and R. P. Viswanath, "Large scale synthesis of CdS nanorods and its utilization in photo-catalytic H_2 production," *Nanotechnology*, vol. 17, no. 20, article 038, pp. 5271–5277, 2006.

[12] G. Guan, T. Kida, K. Kusakabe et al., "Photocatalytic H_2 evolution under visible light irradiation on CdS/ETS-4 composite," *Chemical Physics Letters*, vol. 385, no. 3-4, pp. 319–322, 2004.

[13] H. L. Meng, C. Cui, H. L. Shen et al., "Synthesis and photocatalytic activity of TiO_2@CdS and CdS@TiO_2 double-shelled hollow spheres," *Journal of Alloys and Compounds*, vol. 527, pp. 30–35, 2012.

[14] R. Asahi, T. Morikawa, T. Ohwaki, K. Aoki, and Y. Taga, "Visible-light photocatalysis in nitrogen-doped titanium oxides," *Science*, vol. 293, no. 5528, pp. 269–271, 2001.

[15] C. Yu, D. Cai, K. Yang, J. C. Yu, Y. Zhou, and C. Fan, "Sol-gel derived S,I-codoped mesoporous TiO_2 photocatalyst with high visible-light photocatalytic activity," *Journal of Physics and Chemistry of Solids*, vol. 71, no. 9, pp. 1337–1343, 2010.

[16] Z.-D. Meng, M.-M. Peng, L. Zhu, W.-C. Oh, and F.-J. Zhang, "Fullerene modification CdS/TiO_2 to enhancement surface area and modification of photocatalytic activity under visible light," *Applied Catalysis B: Environmental*, vol. 113-114, pp. 141–149, 2012.

[17] S. Ding, X. Yin, X. Lü, Y. Wang, F. Huang, and D. Wan, "One-step high-temperature solvothermal synthesis of TiO_2/sulfide nanocomposite spheres and their solar visible-light applications," *ACS Applied Materials & Interfaces*, vol. 4, no. 1, pp. 306–311, 2012.

[18] H. Labiadh, T. B. Chaabane, L. Balan et al., "Preparation of Cu-doped ZnS QDs/TiO_2 nanocomposites with high photocatalytic activity," *Applied Catalysis B: Environmental*, vol. 144, no. 1, pp. 29–35, 2014.

[19] T. Shanmugapriya, R. Vinayakan, K. G. Thomas, and P. Ramamurthy, "Synthesis of CdS nanorods and nanospheres: shape tuning by the controlled addition of a sulfide precursor at room temperature," *CrystEngComm*, vol. 13, no. 7, pp. 2340–2345, 2011.

[20] Y. Shemesh, J. E. MacDonald, G. Menagen, and U. Banin, "Synthesis and photocatalytic properties of a family of CdS-PdX hybrid nanoparticles," *Angewandte Chemie International Edition*, vol. 50, no. 5, pp. 1185–1189, 2011.

[21] S. Q. Sun and T. Li, "Synthesis and characterization of CdS nanoparticles and nanorods via solvo-hydrothermal route," *Crystal Growth & Design*, vol. 7, no. 11, pp. 2367–2371, 2007.

[22] Z.-D. Meng, T. Ghosh, J.-H. Cho et al., "Effect of AC and Cu_2O from Cu/Cu_2O-AC/TiO_2 composite catalysts on the photocatalytic degradation of MO under visible light," *Journal of the Korean Ceramic Society*, vol. 48, no. 6, pp. 571–576, 2011.

[23] G. Yang, B. Yang, T. Xiao, and Z. Yan, "One-step solvothermal synthesis of hierarchically porous nanostructured CdS/TiO_2 heterojunction with higher visible light photocatalytic activity," *Applied Surface Science*, vol. 283, pp. 402–410, 2013.

[24] B. Jiang, X. Yang, X. Li, D. Zhang, J. Zhu, and G. Li, "Core-shell structure CdS/TiO_2 for enhanced visible-light-driven photocatalytic organic pollutants degradation," *Journal of Sol-Gel Science and Technology*, vol. 66, no. 3, pp. 504–511, 2013.

[25] Y. Xie, Y. Li, and X. Zhao, "Low-temperature preparation and visible-light-induced catalytic activity of anatase F-N-codoped TiO_2," *Journal of Molecular Catalysis A: Chemical*, vol. 277, no. 1-2, pp. 119–126, 2007.

[26] M. Luo, Y. Liu, J. Hu, H. Liu, and J. Li, "One-pot synthesis of CdS and Ni-doped CdS Hollow spheres with enhanced photocatalytic activity and durability," *ACS Applied Materials & Interfaces*, vol. 4, no. 3, pp. 1813–1821, 2012.

[27] M. Luo, Y. Liu, J. Hu, J. Li, J. Liu, and R. M. Richards, "General strategy for one-pot synthesis of metal sulfide hollow spheres with enhanced photocatalytic activity," *Applied Catalysis B: Environmental*, vol. 125, pp. 180–188, 2012.

[28] Y. Liu, L. Chen, J. Hu, J. Li, and R. Richards, "TiO_2 nanoflakes modified with gold nanoparticles as photocatalysts with high activity and durability under near UV irradiation," *Journal of Physical Chemistry C*, vol. 114, no. 3, pp. 1641–1645, 2010.

[29] T. Guohui, F. Honggang, J. Liqiang, X. Baifu, and P. Kai, "Preparation and characterization of stable biphase TiO_2 photocatalyst with high crystallinity, large surface area, and enhanced photoactivity," *Journal of Physical Chemistry C*, vol. 112, no. 8, pp. 3083–3089, 2008.

[30] L. Wu, J. C. Yu, and X. Fu, "Characterization and photocatalytic mechanism of nanosized CdS coupled TiO_2 nanocrystals under visible light irradiation," *Journal of Molecular Catalysis A: Chemical*, vol. 244, no. 1-2, pp. 25–32, 2006.

[31] D. Gonbeau, C. Guimon, G. Pfister-Guillouzo, A. Levasseur, G. Meunier, and R. Dormoy, "XPS study of thin films of titanium oxysulfides," *Surface Science*, vol. 254, no. 1–3, pp. 81–89, 1991.

[32] T. Blasco, M. A. Camblor, A. Corma, and J. Pérez-Pariente, "The state of Ti in titanoaluminosilicates isomorphous with zeolite *β*," *Journal of the American Chemical Society*, vol. 115, no. 25, pp. 11806–11813, 1993.

[33] R. P. Netterfield, P. J. Martin, C. G. Pacey, W. G. Sainty, D. R. McKenzie, and G. Auchterlonie, "Ion-assisted deposition of mixed TiO_2-SiO_2 films," *Journal of Applied Physics*, vol. 66, no. 4, pp. 1805–1809, 1989.

[34] R. Sanjinés, H. Tang, H. Berger, F. Gozzo, G. Margaritondo, and F. Lévy, "Electronic structure of anatase TiO_2 oxide," *Journal of Applied Physics*, vol. 75, no. 6, pp. 2945–2951, 1994.

[35] Z. Chen and Y. J. Xu, "Ultrathin TiO_2 layer coated-CdS spheres core-shell nanocomposite with enhanced visible-light photoactivity," *ACS Applied Materials & Interfaces*, vol. 5, no. 24, pp. 13353–13363, 2013.

[36] Z. Wang, K. Lv, G. Wang, K. Deng, and D. Tang, "Study on the shape control and photocatalytic activity of high-energy anatase titania," *Applied Catalysis B: Environmental*, vol. 100, no. 1-2, pp. 378–385, 2010.

[37] R. Flood, B. Enright, M. Allen et al., "Determination of band edge energies for transparent nanocrystalline TiO_2CdS sandwich electrodes prepared by electrodeposition," *Solar Energy Materials and Solar Cells*, vol. 39, no. 1, pp. 83–98, 1995.

[38] J.-X. Sun, Y.-P. Yuan, L.-G. Qiu et al., "Fabrication of composite photocatalyst g-C_3N_4-ZnO and enhancement of photocatalytic activity under visible light," *Dalton Transactions*, vol. 41, no. 22, pp. 6756–6763, 2012.